Supporting Information for

Design of MoS_2/Graphene van der Waals Heterostructure as Highly Efficient and Stable Electrocatalyst for Hydrogen Evolution in Acidic and Alkaline Media

Xianbo Yu,[†] Guangyu Zhao,[,‡] Shan Gong,[†] Chao Liu,[†] Canlong Wu,[†] Pengbo Lyu,*[,§] Guillaume Maurin,[§] and Naiqing Zhang*[,‡]*

† School of Chemistry and Chemical Engineering, Harbin Institute of Technology, Harbin, Heilongjiang, 150001, China

‡ Interdisciplinary Science Research Center, Harbin Institute of Technology, Harbin, Heilongjiang, 150001, China

§ ICGM, CNRS, ENSCM, Univ. Montpellier, Montpellier, 34095, France

∗Corresponding Author

E-mail: Guangyu Zhang (zhaogy810525@gmail.com); Naiqing Zhang (znqmww@163.com); Pengbo Lyu (pengbo.lyu@umontpellier.fr)

Experimental Section

Chemicals

The Graphene oxide (GO) was synthesized by Hummers' method and then allocated to a GO/water homogeneous dispersion with the GO concentration of 1.0 mg mL^{-1}. Moreover, all the relevant reagents in this work were purchase from Shanghai Aladdin biochemical technology co., LTD (China) without further treatment except potassium hydroxide aqueous electrolyte was purified.

Preparation of MoS_2/G HS

The MoS_2/G HS catalyst was synthesized as follows: First, 30 mL of negatively charged GO/water homogeneous was modified by the dispersed mixture solution, which was formed by 360 mg of positively charged polyethyleneimine (PEI) and 20 mL distilled water. After stirred continuously for 24 h, the products (PEI/GO) were centrifuged and washed several times by the distilled water. Second, the obtain PEI/GO dispersed in the 30 mL distilled water with sonicated for 30 min, and then 200 mg $(NH_4)_2MoS_4$ were added into the above mixture solution under vigorous stirring for another 24 h. The relevant solid products were collected by centrifuged and washed with distilled water, and dried through a freeze-drying process. Third, the obtained powder was thermally treated at 450^oC for 2 h and then 750^oC for another 2 h under an H_2/Ar flow. After cooling to room temperature, the MoS_2/G HS was obtained.

Preparation of MoS_2/G MP, G, and MoS_2/G MM

The pure MoS_2 micron particles (MoS_2 MP) and pure G were obtained by directly thermal treatment under an H_2/Ar flow from the $(NH_4)_2MoS_4$ and GO power, respectively. The MoS_2/G MM was synthesized by mechanical mixture of MoS_2 MP and G with the appropriate molar concentration ratios of 82.1:17.9.

Electrochemical Measurements

The electrocatalytic activity measurements were performed by a CHI 660D electrochemical workstation in N_2 saturated 1.0 M KOH and 0.5 M H_2SO_4 solutions. The as-synthesized

catalysts covered on the carbon fiber papers were the working electrode with the mass of 1.5 mg cm^{-2}, and a graphite rod and Ag/AgCl electrode can selected as the counter and reference electrodes, respectively. All current densities presented were corrected against ohmic potential drop. The 1000^{th} cyclic voltammetry curves (CVs) measurement were conducted between 0.2 and –0.28 *vs.* the reversible hydrogen electrode (RHE) in 0.5 M H_2SO_4 solution (0.2 and –0.32 *vs.* RHE in 1.0 M KOH solution) to investigate the stability of MoS_2/G HS. Electrochemical impedance spectroscopy (EIS) were measured in a frequency range from 0.1 Hz to 100 kHz. All the measured potentials were corrected *vs.* RHE by the Nernst equation: $E_{RHE} = E_{Ag/AgCl} + 0.059 \times pH + 0.197$ V.

Structure Characterizations

The crystal structure of catalysts were measured by X-ray diffractometer (PANalytical X'Pert PRO) with Cu Kα radiation (λ = 1.5418 Å) at 40 kV and 40 mA. The morphology and microstructures were characterized by scanning electron microscope (Hitachi SU8010, 15 kV) and transmission electron microscopy (Tecnai G2 F30, 200 kV). X-ray photoelectron spectroscopy and Raman spectra analyses were carried out by using a spectrometer with Al Kα radiation (Nepean, ON) and Renishaw INVIA. The contact angle was measured by the instrument from POWEREACH (JC2000D5, 220V).

Computational details

DFT calculations were performed using the projector augmented wave (PAW) formalism within the generalized gradient approximation (GGA) method with Perdew-Burke-Ernzerhof (PBE) exchange-correlation functional as implemented in Vienna Ab Initio Simulation Package (VASP).[1] The cutoff energy of 500 eV for the plane-wave basis set has been consistently used in all calculations. The convergence criterion of 0.05 eV/Å was used for the forces in geometry optimizations and 10^{-4} eV was used for the energy convergence. The rev-vdW-DF2 method proposed by Hamada was employed to include the dispersion contribution for the adsorption.[2] According to experimental observation, the pristine 2H-MoS_2 has the lattice parameters of

a=3.16 Å and *c*=12.29 Å.[3] In this work, the lattice parameters of 2H-MoS_2 unit cell optimized with a 10×10×3 Monkhorst-Pack grid were *a*=3.17 Å and *c*=12.33 Å (interlayer distance 6.17 Å), in good agreement with the experimental values.[4] The lattice parameter of graphene (*a*=2.46 Å) is distinct from MoS_2 by 22%. To construct the heterostructure of MoS_2 and graphene, a 4×4 supercell of MoS_2 and a 5×5 supercell of graphene were used. The difference of lattice parameters then reduced to 3%. Considering the experimental interlayer distance was determined to be 11 Å for the heterostructure in this work, the *c* vector was fixed to 22 Å (double the interlayer distance) during the optimization while *a* vector was relaxed; the optimized *a* vector of the heterostructure was 12.43 Å. The vaccum for the edge model was set to be at least 10Å.

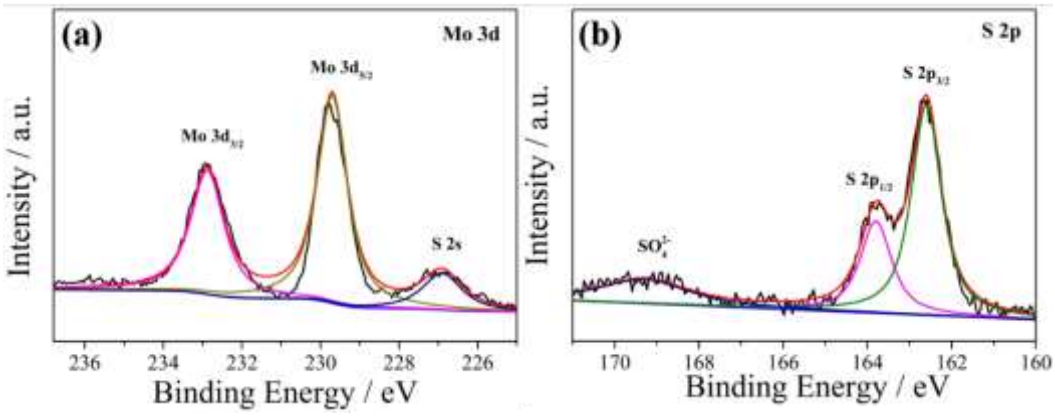

Figure S1. XPS spectra of Mo 3d (a) and S 2p (b) in MoS_2/G HS electrodes toward HER.

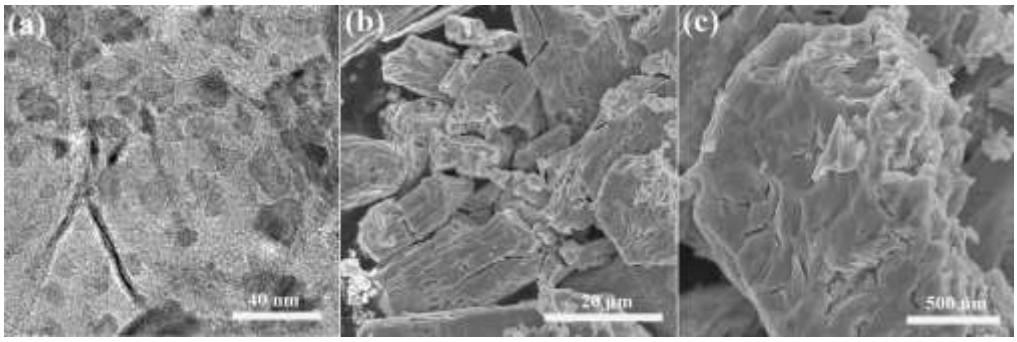

Figure S2. (a) Low-resolution TEM image of MoS_2/G HS, (b-c) SEM images of MoS_2 MP.

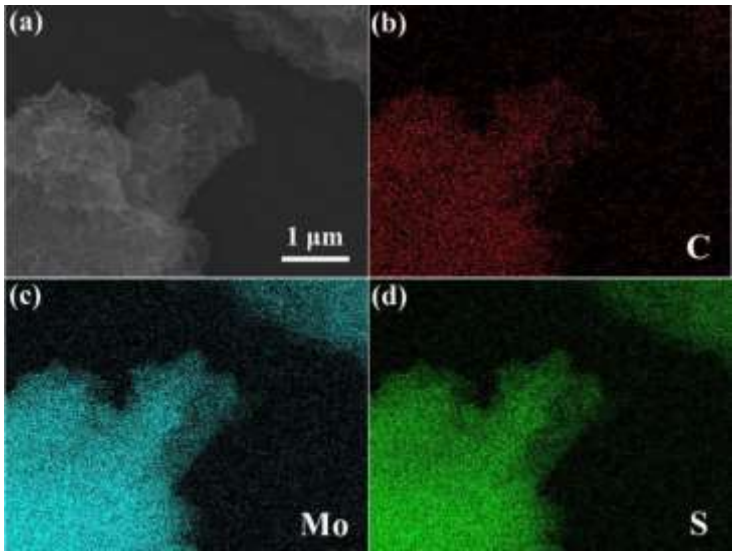

Figure S3. (a-d) Element mapping images of C, Mo, S in MoS_2/G HS.

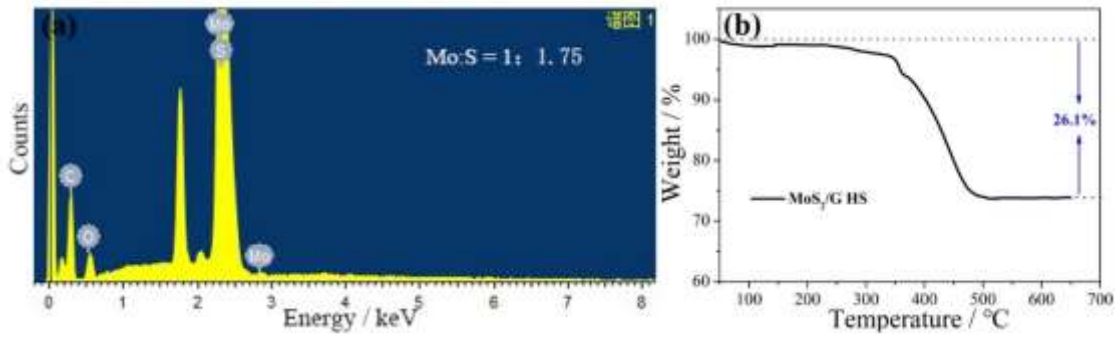

Figure S4. (a) EDS image and (b) TG curve of MoS_2/G HS.

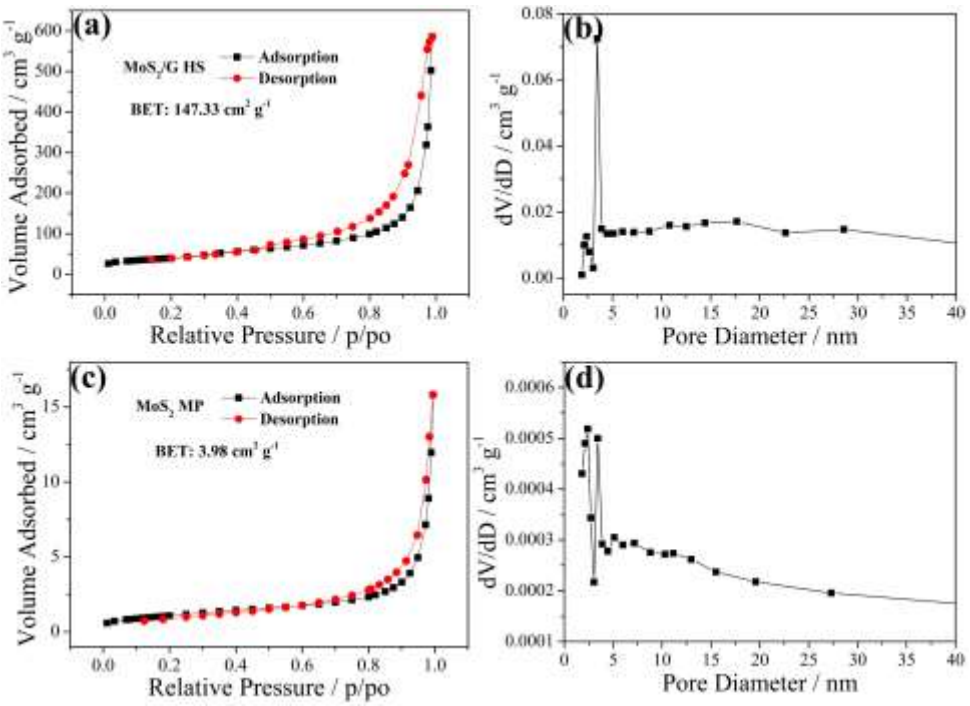

Figure S5. (a, c) Nitrogen adsorption and desorption isotherms and (b, d) the corresponding pore-size distribution calculated of MoS_2/G HS and MoS_2 MP.

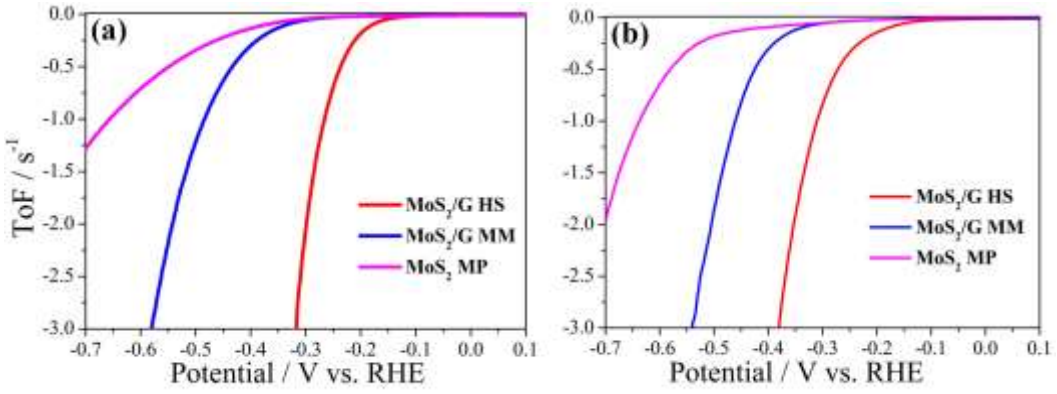

Figure S6. Calculated turnover frequencies for MoS_2/G HS electrode films in (a) 0.5 M H_2SO_4 and (b) 1.0 M KOH solutions.

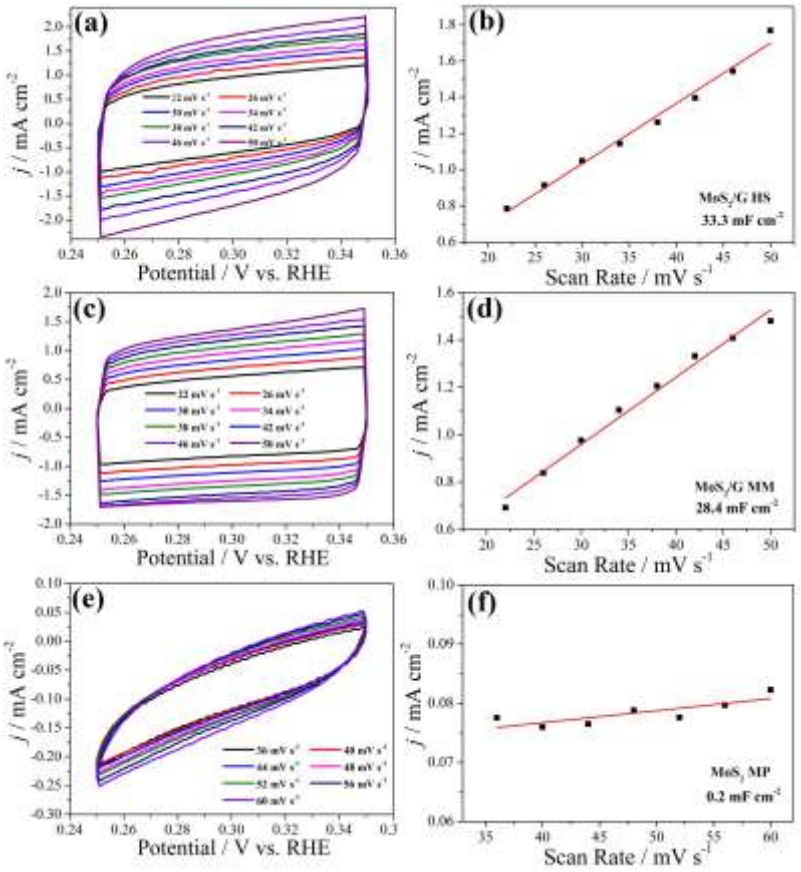

Figure S7. Cyclic voltammograms in the region of 0.25–0.35 V *vs.* RHE for (a) MoS_2/G HS, (c) MoS_2/G MM and (e) MoS_2 MP electrodes. The differences in current density at 0.3 V *vs.* RHE plotted against scan rate fitted to a linear regression allows for the estimation of C_{dl} for (b) MoS_2/G HS, (d) MoS_2/G MM and (f) MoS_2 MP electrodes.

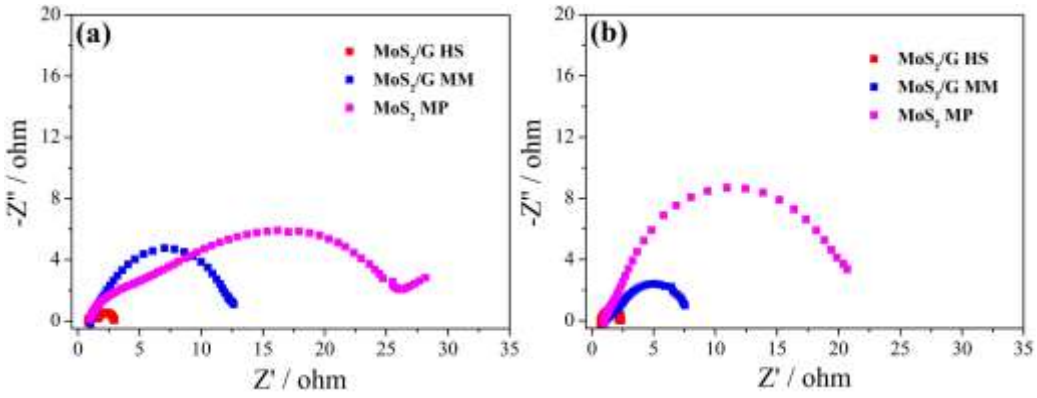

Figure S8. Nyquist plots for MoS_2/G HS, (d) MoS_2/G MM and (f) MoS_2 MP electrodes for HER in (a) 0.5 M H_2SO_4 solution under the overpotentials of 300 mV and b) 1.0 M KOH solution under the overpotentials of 350 mV.

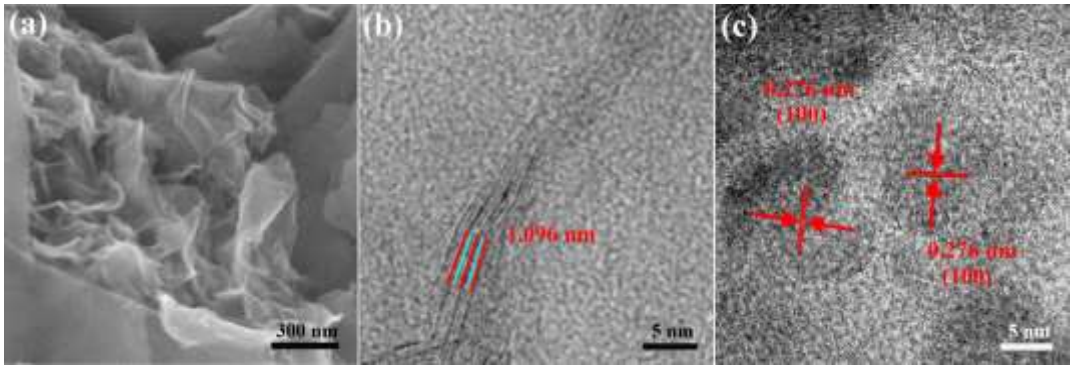

Figure S9. (a) Low-resolution SEM, and (b) HRTEM images of MoS_2/G HS after HER process for 10 h.

Table S1 Comparison of the HER activities of the MoS_2/G HS, MoS_2/G MM, and MoS_2 MP catalysts in 0.5 M H_2SO_4 and 1.0 M KOH solutions with recently published results.

Catalyst	η_{10} (mV)	η_{100} (mV)	Electrolyte	Ref.
Au-MoS_2	280	–	0.5 M H_2SO_4	[5]
MoS_2	187	~240	0.5 M H_2SO_4	[6]
P-doped 2H-MoS_2	217	~320	0.5 M H_2SO_4	[7]
MoS_2 nanodots	248	–	0.5 M H_2SO_4	[8]
MoS_2-cPAN	185	–	0.5 M H_2SO_4	[9]
MoO_2/MoS_2 nanofiber	340	–	0.5 M H_2SO_4	[10]
V-doping MoS_2	194	~275	0.5 M H_2SO_4	[11]
metallic-Phase MoS_2	210	–	0.5 M H_2SO_4	[12]
edge-aligned - 2H/1T-MoS_2/RGO	186	~230	0.5 M H_2SO_4	[13]
amorphous phosphorus-doped MoS_2	219	–	0.5 M H_2SO_4	[14]
oxygen-incorporated MoS_2	~185	~290	0.5 M H_2SO_4	[15]
defect-rich MoS_2	~190	–	0.5 M H_2SO_4	[16]
Co-BDC/MoS_2	248	–	1.0 M KOH	[17]
1T-2H MoS_2 Heterostructures	~280	–	1.0 M KOH	[18]
$Ni(OH)_2$/MoS_2	227	–	1.0 M KOH	[19]

MoS_2 MP	383	675	0.5 M H_2SO_4	This work
	436	647	1.0 M KOH	
MoS_2/G MM	343	494	0.5 M H_2SO_4	This work
	348	468	1.0 M KOH	
MoS_2/G HS	180	268	0.5 M H_2SO_4	This work
	183	313	1.0 M KOH	

References

(1) Perdew, J. P.; Burke, K.; Ernzerhof, M. Generalized Gradient Approximation Made Simple. *Phys. Rev. Lett.* **1996**, *77*, 3865−3868.

(2) Hamada, I. Van der Waals Density Functional Made Accurate. *Phys. Rev. B* **2014**, *89*, 121103.

(3) Jellinek, F.; Brauer, G.; MÜLler, H. Molybdenum and Niobium Sulphides. *Nature* **1960**, *185*, 376.

(4) Monkhorst, H. J.; Pack, J. D. Special Points for Brillouin-Zone Integrations. *Phys. Rev. B* **1976**, *13*, 5188−5192.

(5) Zhao, S.; Jin, R.; Song, Y.; Zhang, H.; House, S. D.; Yang, J. C.; Jin, R. Atomically Precise Gold Nanoclusters Accelerate Hydrogen Evolution over MoS_2 Nanosheets: The Dual Interfacial Effect. *Small* **2017**, *13*, 1701519.

(6) Lukowski, M. A.; Daniel, A. S.; Meng, F.; Forticaux, A.; Li, L.; Jin, S. Enhanced Hydrogen Evolution Catalysis from Chemically Exfoliated Metallic MoS_2 Nanosheets. *J. Am. Chem. Soc.* **2013**, *135*, 10274−10277.

(7) Huang, X.; Leng, M.; Xiao, W.; Li, M.; Ding, J.; Tan, T. L.; Lee, W. S. V.; Xue, J. Activating Basal Planes and S-Terminated Edges of MoS_2 toward More Efficient Hydrogen Evolution. *Adv. Funct. Mater.* **2017**, *27*, 1604943.

(8) Benson, J.; Li, M.; Wang, S.; Wang, P.; Papakonstantinou, P. Electrocatalytic Hydrogen Evolution Reaction on Edges of a Few Layer Molybdenum Disulfide Nanodots. *ACS Appl. Mater. Interfaces* **2015**, *7*, 14113−14122.

(9) Zeleke, T. S.; Tsai, M.-C.; Weret, M. A.; Huang, C.-J.; Birhanu, M. K.; Liu, T.-C.; Huang, C.-P.; Soo, Y.-L.; Yang, Y.-W.; Su, W.-N.; Hwang, B.-J. Immobilized Single Molecular Molybdenum Disulfide on Carbonized Polyacrylonitrile for Hydrogen Evolution Reaction. *ACS Nano* **2019**, *13*, 6720−6729.

(10) Rheem, Y.; Han, Y.; Lee, K. H.; Choi, S.-M.; Myung, N. V. Synthesis of Hierarchical MoO_2/MoS_2 Nanofibers for Electrocatalytic Hydrogen Evolution. *Nanotechnology* **2017**, *28*, 105605.

(11) Bolar, S.; Shit, S.; Kumar, J. S.; Murmu, N. C.; Ganesh, R. S.; Inokawa, H.; Kuil, T. Optimization of Active Surface Area of Flower Like MoS_2 Using V-Doping Towards Enhanced Hydrogen Evolution Reaction in Acidic and Basic medium. *Applied Catalysis B: Environmental* **2019**, *254*, 432−442.

(12) Wang, J.; Wang, N.; Guo, Y.; Yang, J.; Wang, J.; Wang, F.; Sun, J.; Xu, H.; Liu, Z.-H.; Jiang. R. Metallic-Phase MoS_2 Nanopetals with Enhanced Electrocatalytic Activity for Hydrogen Evolution. *ACS Sustainable Chem. Eng.* **2018**, *6*, 13435−13442.

(13) You, B.; Jiang, N.; Sheng, M.; Yano, J.; Sun, Y. High-Performance Overall Water Splitting Electrocatalysts Derived from Cobalt-Based Metal-Organic Frameworks. *Chem. Mater.* **2015**, *27*, 7636−7642.

(14) Wang, D.; Xie, Y.; Wu, Z. Amorphous Phosphorus-Doped MoS_2 Catalyst for Efficient Hydrogen Evolution Reaction. *Nanotechnology* **2019**, *30*, 205401.

(15) Xie, J.; Zhang, J.; Li, S.; Grote, F.; Zhang, X.; Zhang, H.; Wang, R.; Lei, Y.; Pan, B.; Xie, Y. Controllable Disorder Engineering in Oxygen-Incorporated MoS_2 Ultrathin Nanosheets for Efficient Hydrogen Evolution. *J. Am. Chem. Soc.* **2013**, *135*, 17881−17888.

(16) Xie, J.; Zhang, H.; Li, S.; Wang, R.; Sun, X.; Zhou, M.; Zhou, J.; Lou, X. W.; Xie, Y. Defect-Rich MoS_2 Ultrathin Nanosheets with Additional Active Edge Sites for Enhanced Electrocatalytic Hydrogen Evolution. *Adv. Mater.* **2013**, *25*, 5807–5813.

(17) Zhu, D.; Liu, J.; Zhao, Y.; Zheng Y.; Qiao, S. Engineering 2D Metal-Organic Frameworks/MoS_2 Interface for Enhanced Alkaline Hydrogen Evolution. *Small* **2019**, *15*, 1805511.

(18) Wang, S.; Zhang, D.; Li, B.; Zhang, C.; Du, Z.; Yin, H.; Bi, X.; Yang, S. Ultrastable In-Plane 1T-2H MoS_2 Heterostructures for Enhanced Hydrogen Evolution Reaction. *Adv. Energy Mater.* **2018**, *8*, 1801345.

(19) Zhao, G.; Lin, Y.; Rui, K.; Zhou, Q.; Chen, Y.; Dou, S. X.; Sun, W. Epitaxial Growth of $Ni(OH)_2$ Nanoclusters on MoS_2 Nanosheets for Enhanced Alkaline Hydrogen Evolution Reaction. *Nanoscale* **2018**, *10*, 19074–19081.